Journal of Colloid and Interface Science 679 (2025) 975–987

Contents lists available at ScienceDirect

Journal of Colloid And Interface Science

journal homepage: www.elsevier.com/locate/jcis

Regular Article

Lipid nanoparticles as nano-Trojan-horses for siRNA delivery and gene-knockdown

Natalia Sánchez-Arribas [a], Brenda Velasco Rodríguez [b], Emilio Aicart [a], Andrés Guerrero-Martínez [a], Elena Junquera [a,*], Pablo Taboada [b,**]

[a] Dpto. Química Física, Fac. CC. Químicas, Universidad Complutense de Madrid, Av. Complutense s/n, 28040 Madrid, Spain
[b] Departamento de Física de Partículas-Facultad de Física, Instituto de Materiales (IMATUS) e Instituto de Investigaciones Sanitarias (IDIS), Universidad de Santiago de Compostela, Campus Vida, E-15782 Santiago de Compostela, Spain

GRAPHICAL ABSTRACT

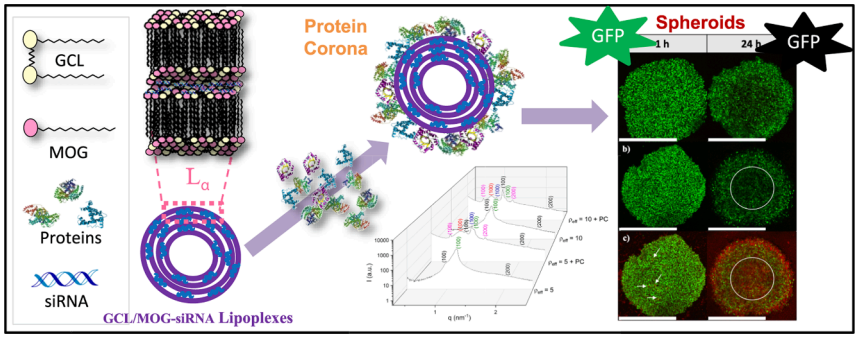

ARTICLE INFO

Keywords:
Lipid-based nanovector
Lipid nanoparticles
Gene knockdown
siRNA
Internalization route
Reactive oxygen species
3D cell spheroids
Cytotoxicity
Lamellar phase

ABSTRACT

The therapeutic messenger RNA strategies, such as those using small interfering RNAs, take several advantages (versatility, efficiency and selectivity) over plasmid DNA-based strategies. However, the challenge remains to find nanovectors capable of properly loading the genetic material, transporting it through troublesome environments, like a tumoral site, and delivering it into the cytoplasm of target cells. Here, lipid nanoparticles, consisting of a gemini cationic/neutral helper lipid mixture, are proposed as siRNA nanovector. Cells from cervical and brain cancer overexpressing the green fluorescent protein (GFP) were chosen to analyse the biological response as well as the efficiency and safety of the siRNA-loaded nanovector according to the cell phenotype. Flow cytometry and epifluorescence or confocal microscopy were used to follow the gene knockdown in these overexpressed cells. The effect of the nanovector on cellular proliferation was evaluated with cytotoxicity assays while their potential oxidative stress generation was determined by quantifying the generation of reactive oxygen species. To explore the mechanism of cellular uptake, different inhibitors of endocytic pathways were used during incubation with cells. Finally, nanovectors were incubated in 3D-grown cells (spheroids) to see

* Corresponding author at: NanoPhysical Chemistry Group, Faculty of Chemistry, Department of Physical Chemistry, Universidad Complutense de Madrid, Ciudad Universitaria s/n, 28040 Madrid, Spain.
** Corresponding author at: Colloids and Polymer Physics Group (GFCP), Condensed Matter Physics Area, Faculty of Physics, Universidade de Santiago de Compostela, 15782 Campus Vida, Santiago de Compostela, Spain.
E-mail addresses: junquera@ucm.es (E. Junquera), pablo.taboada@usc.es (P. Taboada).

https://doi.org/10.1016/j.jcis.2024.10.115
Received 20 June 2024; Received in revised form 17 October 2024; Accepted 19 October 2024
Available online 22 October 2024

whether they can penetrate the complex tumoral microenvironments, their efficiency to knockdown GFP expression being monitored by confocal microscopy.

1. Introduction

In recent decades, gene therapy has emerged as a promising treatment strategy for a variety of genetic and acquired diseases [1,2]. In particular, interfering RNAs (RNAi) constitute a forefront approach in molecular biology for gene silencing, enabling targeted modulation of gene expression at the post-transcriptional level. Unlike DNA, which must reach the nucleus to perform a predesigned activity, RNAi strategies include the use of double-stranded RNA (dsRNA) or shorter interfering RNA (siRNA) sequences to offer a highly specific means to interfere with messenger RNA (mRNA) translation, inducing efficacious post-transcriptional silencing of the gene of interest with high specificity [3,4]. Nonetheless, siRNA molecules (ranging from 21 to 23 nucleotides) face challenges in crossing the cell membrane easily and are susceptible to rapid degradation by serum nucleases. Additionally, similar as plasmid DNA, the negative charge of RNAs hinders their transport through the negatively charged cell membrane. Consequently, the realization of the extensive potential of RNAi-based therapeutics depends on achieving effective delivery of siRNA molecules into target cells through safer delivery vehicles [5–8].

In this context, lipid nanoparticles (LNPs) have emerged in the last decade as versatile and effective nanocarriers, playing a crucial role in overcoming challenges associated with nucleic acid administration [9,10]. The intrinsic ability of lipids to self-aggregate into a wide variety of nanostructures and lyotropic liquid crystalline phases, capable of compacting bioactive molecules to form stable complexes, gives them the ability to cross biological barriers, ensuring internalization into target cells, like true molecular nano-Trojan horses. These lipid nanoaggregates offer several advantages, including biocompatibility, efficient compaction capacity, and the ability to be functionalized to enhance cellular specificity and selectivity [10,11].

Among the myriad cationic lipids (CLs) used in the last decades in the field of nucleic acid delivery, gemini cationic lipids (GCLs) represent a distinct class of amphiphiles that have gained significant attention [12,13]. These molecules are characterized by a unique architecture consisting of two hydrophobic tails with their corresponding positively charged polar heads connected by a rigid or flexible spacer of different characteristics. This distinctive dimeric nature provides a platform for overcoming challenges associated with traditional monomeric cationic lipids, such as toxicity, and limited transfection efficiency. As the field of nucleic acid delivery continues to evolve, GCLs promise to be versatile and efficient nanocarriers for various gene therapy applications, showing their potential impact on advancing the field of personalized medicine. Although in recent research GCLs have demonstrated superior performance in delivering plasmid DNAs (pDNAs) as therapeutic genes [14–19], the use of GCLs for siRNA delivery is a relatively less-explored phenomenon in current research of lipid-based gene delivery.

On the other hand, to construct an efficient gene delivery nanosystem it is also required to analyse how this nanocarrier behaves and interacts within the biological milieu. In particular, for siRNA-based cancer therapy, it is essential to elucidate the ability of the nanovehicle to cross the complex microtumoral environment to reach the targeted diseased cells as well as the mechanisms involved in its internalization within such cells, which would determine the release of the genetic cargo inside the cell cytoplasm for efficient therapeutic action [14,20]. For such purpose, three-dimensional (3D) cell cultures, such as cell spheroids, have emerged as more sophisticated bio tools to model *in vivo* tumour physiology and development [21,22]. Such spheroids are aggregates of cells which allows the improved recapitulation of cell–cell interactions, signalling gradients, and nutrient diffusion, thus, offering a more physiologically relevant environment compared to traditional two-dimensional (2D) cultures while overcoming some of their limitations [23]. Even though this 3D cellular model is grown from monocultures, it still preserves the essential features present in cancer tumours *in vivo*, that is, rapid proliferation at its surface and slow metabolism, or even necrosis, in the centre of the spheroid [24], as well as providing a more complex tumoral microenvironment and structure, which allows the detailed analysis about the capacity of nanocarrier penetration, release of anticancer compounds and subsequent cargo-induced responses into tumoral tissue [25], thus, becoming an intermediate, advanced cell model between traditional 2D cultures and more expensive, ethically-concern animal *in vivo* models.

Following such guidelines, in the present work gene vectors in the form of lipoplexes constituted by a GCL of the bis(hexadecyl dimethyl ammonium) oxyethylene series, referred to as $(C_{16}Am)_2(C_2O)_3$, and mono oleoyl glycerol (MOG) as a neutral helper lipid were prepared with the aim of substantially reducing EGFP expression in EGFP-expressing cell 2D cultures and tumoral spheroids without displaying any noticeable toxicity as a proof concept to get a novel siRNA-based delivery nanocarrier for tumour treatment. It is reported that the presence of a hydrophilic spacer within GCL structure provides a better lipid–nucleic acid interaction and better pDNA transfection results, compared with the GCL bis(hexadecyl diethyl ammonium) alkane series [26,27], but its role in gene silencing has not yet been studied.

Accordingly, the analysis reported in this work are focused on the physicochemical and biological characterization of $(C_{16}Am)_2(C_2O)_3$/MOG-siRNA (from now GCL/MOG-siRNA) lipoplexes as vectors for siRNA delivery and silencing. Despite GCL/MOG-based lipidic surfactants with hydrophilic spacer have been shown to successfully complex pDNA [14], the evident structural differences between the former genetic material and siRNA (pDNA has a size of several kilo bp, while siRNA has only about 21–23 bp) may consequently impact electrostatic interactions with polycations and the ability to form stable complexes as well as their final size, electric surface charge and structure. Then, the lipoplexes here formed were physically characterized by agarose gel electrophoresis, dynamic light scattering (DLS) and ζ-potential techniques, and structurally by small-angle X-ray scattering (SAXS), being demonstrated that protein corona plays a key role in the resulting structure of the derived lipidic-based nanoparticles. The cytotoxicity and ability to generate reactive oxygen species (ROS) of lipoplexes were analysed by means of commercial CCK-8 and ROS assays, respectively, in two cancer cell lines modified to overexpress the green fluorescent protein, GFP, such as human cervical HeLa and mouse astrocytes T731, in order to consider potential differences resulting from different tumoral cell phenotypes. The possible mechanisms involved in the uptake and internalization of dye-stained lipid nanocarriers for the successful delivery of their cargo to cells were analysed by flow cytometry using different inhibitors known to selectively block a specific internalization pathway, being observed that the clathrin-mediated pathway is predominant over others for lipoplex internalization. The former techniques were also used to provide information about the internalization capacity and gene silencing activity by monitoring the cell fluorescence signal in 2D cultures and 3D cell spheroids. With the latter model we aimed to recapitulate the dense and complex tumoral structure and demonstrated that the present lipidic nanocarriers may then reach tumoral cells in such more complex architectures and release the therapeutic cargo on site. Altogether, these experiments could allow us to confirm the potential utility of this lipid GCL/MOG-based nanocarrier for efficient silencing-based therapy.

2. Experimental section

2.1. Materials

The GCL, with formula $(C_{16}Am)_2(C_2H_4O)_3C_2H_4$, was kindly supplied by Prof. S. Bhattacharya (Indian Institute of Science, Bangalore, India) and details of its synthesis and subsequent characterization are already reported in the literature [27]. The helper lipid MOG (Scheme 1b) and Pluronic F127 (10 % solution in water) were supplied by Sigma-Aldrich and Invitrogen-Thermo Fisher (Waltham, MA), respectively.

Dulbecco's modified Eagle's medium (DMEM) was supplied by Hyclone-Thermo Fisher (Waltham, MA), whereas fetal bovine serum (FBS), antibiotics, sodium pyruvate, and non-essential amino acids (NEAAs) were purchased from Gibco-Thermo Fisher (Waltham, MA). Human serum (HS) used as received, ROS-detection kit, and internalization inhibitors (NaN_3, 2-deoxyglucose (DOG), cytochalasin D, dynasore, genistein, methyl-β-cyclodextrin (Mβ-CD, 3 mg/mL) and chlorpromazine were from Sigma-Aldrich. AntiGFP-siRNA ($siRNA_{antiGFP}$) was obtained from Ambion-Thermo Fisher, and the non-targeting control siRNA ($siRNA_{non\text{-}targeting}$) and commercial control Lipo2000* (Lipofectamine2000* transfection reagent) were supplied by Invitrogen-Thermo Fisher. HeLa-GFP cervical cancer cells were purchased from Cell Biolabs (San Diego, CA). T731 mice astrocytes were kindly donated by Prof. J. A. Costoya (University of Santiago de Compostela, Spain) and modified for overexpression of GFP (hereafter denoted as T731-GFP), as previously reported [28].

2.2. Preparation of lipoplexes

Dry lipid films, with the corresponding amounts of GCL and MOG to obtain a GCL molar composition in the mixed lipid of α = 0.7, were formed by evaporation of a lipid chloroform solution under high vacuum. These lipid films were hydrated in N-(2-hydroxyethyl)piperazine-N′-ethanesulfonic acid (HEPES)-buffered medium (40 mM, pH = 7.4) and homogenized by alternating vortex/sonication cycles. A sequential extrusion procedure, fully detailed earlier [29] was used to homogenize the size and morphology of the multilamellar lipid mixtures formed after the hydration process and to convert them into unilamellar ones. Subsequently, Pluronic F127 was added to the lipid mixture to provide colloidal stability (0.1 μg/μL to obtain a final concentration of 10 % in mass of CL). Finally, the mixture of cationic and neutral lipids was mixed with the appropriate amount of siRNA solution to obtain specific molar charge effective ratios of ρ_{eff} = 5 and 10 to form the lipoplexes (see Supporting Information for details of the protocol for the determination of effective charges and effective charge ratios, ρ_{eff}). The siRNA stock solution varied depending on the technique of analysis: 0.1 mg/mL for ζ-potential, 0.2 μg/well (0.1 mg/mL) for agarose gel electrophoresis, 50 μg/capillary (10 mg/mL) for SAXS, and 5 nmol/mL (antiGFP-siRNA, denoted as $siRNA_{antiGFP}$) or 1 nmol/mL (non-targeting siRNA, denoted as $siRNA_{non\text{-}targeting}$) for biological experiments.

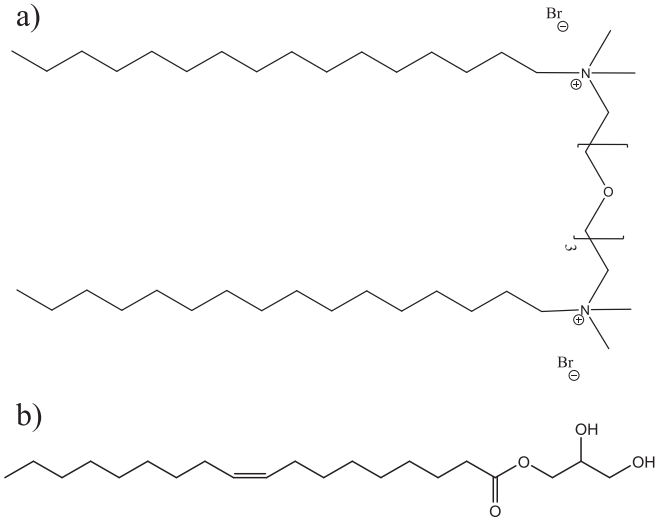

Scheme 1. Molecular structure of (a) the GCL and (b) the neutral lipid MOG.

2.3. Physicochemical characterization

2.3.1. ζ-potential, particle size and polydispersity

The phase analysis light scattering technique (Zeta PALS, Brookhaven Instruments Corp., Holtsville, USA) was used to measure the electrophoretic mobility of GCL/MOG-siRNA lipoplexes, from which the ζ-potential was obtained using a dispersant refractive index of 1.33 (water), viscosity of 0.9 cP, dispersant dielectric constant of 78.5 and temperature of 25 °C. The particle size of lipoplexes, as well as the polydispersity index (PDI), were determined from dynamic light scattering (DLS) measurements carried out with the same equipment. The three properties (ζ-potential, particle size and polydispersity) were calculated each from the average of 50 (ζ-potential) and 30 (particle size and polydispersity) independent measurements, respectively, and collected as a function of the mass ratio content between the lipid mixture and siRNA, m_L/m_{siRNA}, or effective charge ratio (ρ_{eff}), given by Eqs. (1) and (2)

$$m_L/m_{siRNA} = \left(m_{GCL} + m_L^0\right)/m_{siRNA} \tag{1}$$

where m_L, m_{GCL}, m_L^0, and m_{siRNA} are the masses of the total mixed lipid, the GCL, the neutral lipid (MOG), and siRNA, respectively, and

$$\rho_{eff} = \frac{n^+}{n^-} = \frac{q^+_{eff,\,GCL}\left(m_{GCL}/M_{GCL}\right)}{q^-_{eff,\,siRNA}\left(m_{siRNA}/M_{siRNA}\right)} \tag{2}$$

where n^+, n^-, $q^+_{eff,GCL}$, $q^-_{eff,siRNA}$, M_{GCL} and M_{siRNA} are the number of moles of positive (GCL) and negative (siRNA) charges, effective charges of GCL and siRNA per bp, and the molecular weight of GCL and siRNA per bp, respectively (see Supporting Information for details).

2.3.2. Agarose gel electrophoresis

This technique was used to determine the extent of siRNA complexation and compaction by the lipid mixture of GCL and MOG. Free siRNA and the lipoplexes were included in gels formed by 0.8 % (w/v) agarose in 1X TAE buffer, and 0.7 μL of GelRed probe. Electrophoresis was run at room temperature (around 25 °C) at 70 mV for 1 h. The samples were excited at 302–312 nm and recorded at 600 nm. The corresponding emission bands were visualized using the commercial Quantity One software and a Gel Doc XR instrument (Bio-Rad). Free RNA exhibits a characteristic fluorescent band down the lane, while the absence of such a band confirms the siRNA complexation and compaction by the mixed lipid

2.3.3. Small-angle X-ray scattering (SAXS)

SAXS was used to determine the structure of the lipoplexes. To do that, SAXS experiments were performed at the ALBA Synchrotron (Barcelona, Spain, beamline BL11) using 12.6 KeV (λ = 0.995 Å) as the energy of the incident beam and a Quantum 210r CCD detector. Scattered X-rays were converted into one-dimensional scattering by radial averaging and plotted as a function of the momentum transfer vector (q) in the diffractograms. GCL/MOG-siRNA lipoplexes were formed at two different effective charge ratios (ρ_{eff} = 5 and 10) with and without HS (10 % v/v) in the capillaries. Samples were measured in duplicate at each composition

2.4. Cell culture conditions

All cells were maintained at 37 °C under 5 % CO_2 (standard culture

conditions) in DMEM supplemented with 10 % (v/v) FBS or HS (for the incubation of the lipoplexes in cells), 1 % (v/v) penicillin/streptomycin, 1 % (v/v) sodium pyruvate, and 1 % (v/v) non-essential amino acids (NEAAs).

2.5. Cell viability

The cytotoxicity of GCL/MOG-siRNA lipoplexes was determined in both GFP-overexpressing HeLa and T731 cell lines using the Cell Counting Kit-8 (CCK-8) assay. In 96-well plates, GFP-modified cells were seeded (100 μL, 10,000 cells/well) and incubated for 24 h. Afterwards, lipoplexes formed by lipid mixtures at $\rho_{eff} = 5$ and 10 and 5 pmol/well of $siRNA_{non\text{-}targeting}$ were incubated for 48 and 72 h in the presence of 10 % (v/v) of HS. Next, the medium was discarded, the cells were washed with 10 mM phosphate-buffered saline (PBS), and 10 μL of the CCK-8 reagent was added to each well with 90 μL of fresh culture medium. Lipo2000* (0.25 μL/well) was used as the positive control for transfection and non-treated cells as the negative one. A UV–vis microplate absorbance reader (Bio-Rad, model 689) was used to measure the absorbance of the samples and non-treated cells at 450 nm. The percentage of cell viability was then calculated using the following equation: $A_{sample}/A_{untreated}$ cells × 100.

2.6. Reactive oxygen species (ROS) activity

A fluorometric intracellular ROS kit (Sigma-Aldrich, USA) was used to detect ROS according to manufacturer's instruction. Briefly, 20,000 HeLa cells/well were seeded on 96-well plates with 100 μL of DMEM without red phenol and grown for 24 h at standard culture conditions. Afterwards, 100 μL of GCL/MOG-siRNA lipoplexes formed by lipid mixtures at $\rho_{eff} = 5$ and 10 and 5 pmol/well of $siRNA_{non\text{-}targeting}$ were added to the wells and incubated for 4 h. Then, the medium was discarded, cells were washed three times with PBS and, finally, fresh culture medium without red phenol was added. Then, 100 μL of ROS detection reagent were added to each well and cells were incubated for 1 h at 37 °C and its fluorescence measured using a microplate reader ($\lambda_{ex} = 520$ nm; $\lambda_{em} = 605$ nm). As a negative control some cells were left untreated (without lipoplexes), and as a positive control 100 % ROS was induced by adding in this step H_2O_2 (800 μM, 33 % (w/v)).

2.7. Uptake inhibition studies

GFP-modified cells were seeded (1 mL, 40,000 cells/well) in 12-well plates and incubated for 24 h at standard culture conditions. After that, cells were treated with 0.1 % NaN_3/50 mM 2-deoxyglucose (DOG), cytochalasin D (15 μg/mL), dynasore (140 μg/mL), genistein (54 μg/mL), methyl-β-cyclodextrin (Mβ-CD, 3 mg/mL) and chlorpromazine (14 μg/mL) in serum-free DMEM for 1 h. Then, cells were washed and incubated with the GCL/MOG-siRNA lipoplexes doped with Nile Red (200:1 lipid:probe molar ratio) and formed at $\rho_{eff} = 10$ (40 pmol/well of $siRNA_{non\text{-}targeting}$) in the fresh media for 4 h at 37 °C/5 % CO_2. The medium was then changed to fresh media. Cellular internalization was analysed after 72 h of incubation, where cells were trypsinized and processed for flow cytometry.

2.8. In vitro gene knockdown efficiency

Flow cytometry and epifluorescence or confocal microscopy were used to evaluate the gene knockdown activity of the GCL/MOG-siRNA lipoplexes after 48 and 72 h of incubation with the tumoral cell lines.

2.8.1. Flow cytometry

For flow cytometry experiments, 12-well plates were used to seed GFP-expressed cells (2 mL, 40,000 cells/well). After 24 h of incubation, the GCL/MOG-siRNA lipoplexes formed by 40 pmol/well of $siRNA_{antiGFP}$ and the corresponding lipid mixture to reach specific effective charge ratios ($\rho_{eff} = 5$ and 10) and doped with Nile red (200:1 lipid:probe molar ratio) were incubated with cells in the presence of 10 % of HS. Untreated GFP-expressed cells, $siRNA_{non\text{-}targeting}$ inserted with 2 μL/well of Lipo2000*, and $siRNA_{antiGFP}$ inserted freely and with 2 μL/well of Lipo2000* were used as controls under the same conditions. After 48 and 72 h, the cells were harvested with trypsin and suspended in 200 μL of PBS after several washes at 1200 rpm for 4 min. The average fluorescence intensity per cell (mean fluorescence intensity, MFI) was determined using a Guava easyCyte HT System flow cytometer and GuavaSoft software for 5000 events (cell count). The GFP down-regulation was analyzed based on the average of fluorescence intensity per cell (MFI) and on the percentage of cells expressing GFP (%GFP)

2.8.2. Epifluorescence microscopy analysis

The gene knockdown activity was also studied by epifluorescence microscopy. Cells overexpressing GFP were seeded on poly-L-lysine-coated glass coverslips (76 mm × 26 mm), placed inside 6-well plates (3 mL, 100,000 cells/well), and grown for 24 h under standard cell culture conditions. The GCL/MOG-siRNA lipoplexes were formed by a lipid mixture at $\rho_{eff} = 5$ and 10 plus 100 pmol/well of $siRNA_{antiGFP}$. With 5 μL/well of Lipo2000*, $siRNA_{antiGFP}$ was inserted and used as positive control, under similar conditions. After 72 h incubating the lipoplexes in the presence of cells, they were washed with PBS, fixed with paraformaldehyde 4 % (w/v) for 10 min, permeabilized with 0.2 % (w/v) Triton X-100 for 10 min, and cytoplasm-stained for 20 min with Alexa Fluor 647 (Invitrogen-Thermo Fisher), with PBS washes between steps. Then, the coverslips were mounted on glass slides, and the nuclei were stained with 4′,6-diamidino-2-phenylindole (DAPI; Invitrogen-Thermo Fisher). The GFP expression levels were visualized after storage of the cells at −20 °C for at least 24 h using an epifluorescence microscope (Leica DMI6000B) with a Leica AF6000 modular system and a DFC3665FX camera (Leica Microsystems GmbH, Heidelberg, Mannheim, Germany) equipped with an oil 63x objective. The blue channel was used for DAPI ($\lambda_{ex} = 350$ nm), the green channel for GFP ($\lambda_{ex} = 520$ nm), the far-red channel for Alexa Fluor 647 ($\lambda_{ex} = 650$ nm), and transmitted light was employed in differential interference contrast mode. The analysis of the fluorescence intensities was performed using LAS X Life Science and ImageJ software packages following a previously established methodology [30] to do that, regions of interest (ROIs) considering well-defined cells were selected in different microscopic images at selected time points and the fluorescent signal was normalized and quantified regarding the signal background and suitable controls (initial fluorescent cell spheroids and lipoplexes)

2.8.3. Confocal microscopy analysis

The gene knockdown activity was also studied by confocal microscopy in 3D cell (spheroids) cultures. For spheroid formation, 96-well plates were coated with 70 μL of a 1 % agarose (w/v) solution in sterile water. During the coating process, the agarose solution was maintained at 70 °C followed by cooling and setting at room temperature for 40 min [31]. Then, HeLa and T731 GFP-modified cells were seeded (100 μL, 20,000 cells/well) and incubated for 24 h to form the spheroid. After that, the GCL/MOG-siRNA lipoplexes formed by 40 pmol/well of $siRNA_{antiGFP}$ and the corresponding lipid mixture modified with Nile Red (200:1 final molar ratio) to reach specific effective charge ratios ($\rho_{eff} = 10$) were incubated with the spheroids in the presence of 10 % of HS. Untreated cells were used as controls. Confocal microscopy images were collected using a Leica Stellaris 8 FALCON inverted confocal laser scanning microscope (Leica Microsystems, Germany) equipped with Leica Application Suite X (LAS X) and at 1, 24, and 48 h of GCL/MOG-siRNA lipoplexes incubation. Spheroids were excited with a white light laser (WLL2). The excitation/emission wavelengths were set at 473/478–550 nm for GFP and 553/577–700 for Nile Red, respectively. Hybrid detectors were used to collect the fluorescent light emission. A series of images (x-y-z) were acquired in sequential mode with a resolution of 1024 × 1024 pixels, corresponding to an x-y area od 1.5 mm ×

1.5 mm at z-intervals of 5 μm, using an HC PL APO CS2 10×/0.4 dry objective

2.9. Statistical analysis

Statistical analysis of experimental data was performed with Origin software. All results were presented as mean standard deviation unless otherwise stated. Unpaired *t*-test (*P < 0.05; **P < 0.01, ***P < 0.005) was used to determine statistical differences in individual groups.

3. Results and discussion

The capacity and efficiency of lipoplexes to act as nano-Trojan-horses able to deliver genetic material into the cells relies on a packing-unpacking mechanism conducted by the lipid mixture, which is responsible for the compaction, in the present case, of siRNA and its subsequent transport and delivery inside the cells. The net charge, size, and polydispersity of the lipoplex, their capacity to compact the siRNA molecule and their physiological stability, as well as their ability to be internalized into cells by a single or a combination of pathways, which enable an effective siRNA release into the cell cytoplasm, are among the most decisive factors to favor a successful transfection process [32].

In this work, GCL/MOG-siRNA$_{non\text{-}targeting}$ lipoplexes at α = 0.7 resulted in an outstanding complexation of the siRNA material as here demonstrated by both the inversion of the initial negative electric charge of the non-compacted nucleic acid to positive after compaction (ca. +25.0 mV), that is, when the lipoplex nanocarrier is formed (Fig. 1a), and the absence of any free siRNA chains in solution once the electroneutrality of the lipoplex is overcome, as seen by agarose gel electrophoresis (Fig. 1b, lanes 3 and 4). In this regard, a Boltzmann-type fit of the data in Fig. 1a allowed to determine the electroneutrality ratio of the GCL/MOG-siRNA$_{non\text{-}targeting}$ lipoplexes at $(m_L/m_{siRNA})_\phi$ = 2.2 ± 0.2. Using a protocol fully described previously [27,29] (see Supporting Information for details) the effective charge of GCL was calculated to be 1.50 ± 0.15, which was a 25 % lower than the nominal one (+2). This decrease of the effective charge with respect to the nominal one, already seen in the literature [29,33–36] is characteristic for lipids with substituted quaternary ammonium cationic head groups.

To analyse the potential of the developed GCL-based lipoplex nanocarriers for the efficient transport and delivery of siRNA into cells for therapeutic purposes, their biocompatibility must be firstly ensured. For such, a colorimetric assay (CCK-8) was used to evaluate the potential cell cytotoxicity induced by scrambled siRNA-loaded lipoplexes (GCL/MOG-siRNA$_{non\text{-}targeting}$) in two different cell cultures, human tumoral

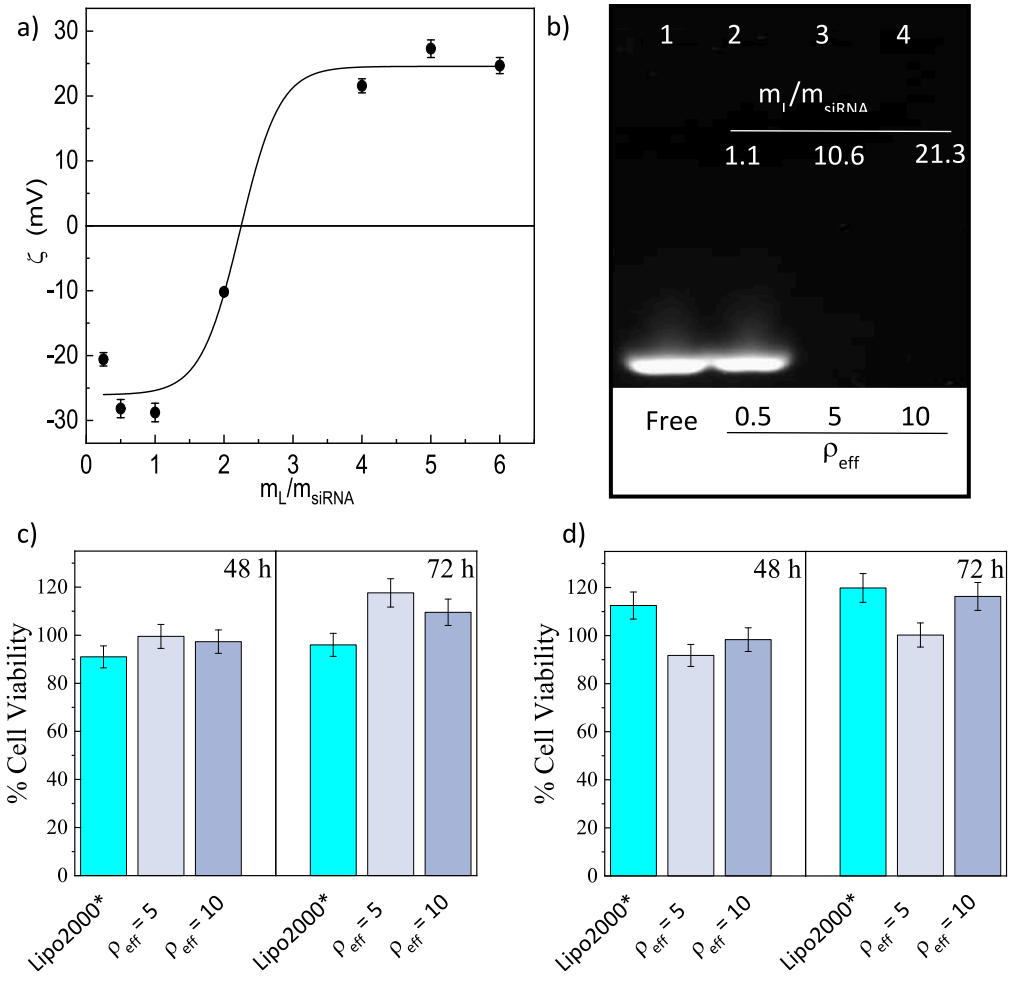

Fig. 1. (a) Plot of the ζ vs. mass ratio (m_L/m_{siRNA}) of GCL/MOG-siRNA$_{non\text{-}targeting}$ lipoplexes at α = 0.7 Data represent the average of 50 independent measurements of ζ, with an uncertainty of ±5 %; (b) Agarose gel electrophoresis of the lipoplexes formed at selected m_L/m_{siRNA} (or ρ_{eff}) (2–4 lanes). Used as control: free siRNA (lane 1); Cell viability of HeLa-GFP (c) and T731-GFP (d) cell lines in the presence of GCL/MOG-siRNA$_{non\text{-}targeting}$ lipoplexes at α = 0.7 and ρ_{eff} = 5 (light gray bars) and 10 (dark grey bars). The % of cell viability was normalized to that obtained for untreated cells. The blue bar corresponds to commercial control Lipo2000*-siRNA$_{non\text{-}targeting}$, used here as positive control. The experiments were performed in the presence of 10 % of HS and at 48 and 72 h post-incubation. The data represent the mean of three wells and uncertainties are within ±5 %. (For interpretation of the references to colour in this figure legend, the reader is referred to the web version of this article.)

cervical HeLa-GFP (Fig. 1c) and mouse T371-GFP astrocytes (Fig. 1d). The lipoplexes were tested at two different compositions, $\rho_{eff} = 5$ and 10, with the aim of finding the optimal lipoplex composition where they are highly efficient in silencing and minimally cytotoxic (see Supporting Information for details of the procedure to determine effective charge ratios, ρ_{eff}). The evaluation was done after 48 and 72 h of incubation in the presence of human serum (HS) to configure the biological entity cells would see after their administration (the nanoparticle core plus the adsorbed shell of physiological proteins, i.e., the protein corona).

Under the described conditions (ρ_{eff} = 5 and 10), lipoplex cytocompatibilities above 90 % in both HeLa-GFP and T731-GFP cells were attained in the concentrations range analysed (see Fig. 1c and 1d). Specifically, for HeLa-GFP the cell survival rate was rather larger than that corresponding to lipoplexes made with the commercial Lipo2000* lipid here used as control. This result highlights the importance of cell phenotype to determine the toxicity and biological induced responses of a specific nanocarrier for an envisaged therapeutic application. In addition, it is observed that longer incubation periods after lipoplex administration seem to favour somehow cell proliferation when comparing cell viability data at 48 and 72 h post-incubation. On the basis of the present experimental data, the present LNPs can be then considered as safe and biocompatible. Such high biocompatibility observed for GCL/MOG-siRNA$_{non\text{-}targeting}$ lipoplexes agrees with that previously reported for other lipid-based nanocarriers containing amino acid moieties in their cationic heads used for genetic material delivery [37–39], which confirms the interest of this class of nanocarriers for intended drug delivery applications and, in particular, for gene therapy.

Apart from toxic effects which may directly affect cell structure and/or metabolism, the administration of exogenous nanomaterials cannot only involve additional cell biological responses which can induce programmed cell death pathways [40], but also to activate or deactivate a variety of receptors, proteins, ions, and other signalling molecules involved with deleterious biological processes [41]. Here, the potential oxidative stress generated after the administration of GCL/MOG-siRNA$_{non\text{-}targeting}$ lipoplexes at $\alpha = 0.7$ and ρ_{eff} = 5 and 10 to cells was assessed by measuring the concentration of intracellular ROS, particularly, $OH^{\bullet}$ and O_2^{-} radicals, using a fluorometric ROS assay kit. As observed in Fig. S1, the administration of the lipoplexes led to a certain increase in the intracellular ROS concentration in HeLa-GFP cells, particularly at $\rho_{eff} = 10$, compared to those treated with Lipo2000-based lipoplexes. This observation may be related to a slightly larger uptake of the nanocarriers in this cell line compared to T731-GFP, which may be especially favoured by an excess of surface positive charge of the lipoplexes at $\rho_{eff} = 10$. Conversely, no statistically significant differences in ROS production after administration of the present lipoplexes were observed for T731-GFP cells compared to control Lipo2000-based particles. This additionally corroborates the influence of cell phenotype on the potential biological responses of the administered nanocarriers and nanomaterials for drug delivery applications [42–44]. Similar conclusions were also driven by, for example, Kroll et al. who reported quite different cytotoxic responses of 23 types of nanomaterials tested in 10 different cell lines [45]. Xia et al [46] also assessed the cytotoxicity of cationic polystyrene nanospheres in five different cell cultures, finding potential harmful cytotoxic effects in only two of them. Similarly, Fröhlich et al. evaluated the cytotoxicity of 20-nm carboxyl polystyrene particles in 20 types of cells of several species (human, mouse, rat, bovine) with distinct proliferation rates, embryonic origin (epithelial, mesenchymal) and phagocytosis capacity under different growth conditions (in monolayer or in suspension). It was observed that the resulting inhibitory concentrations (IC50) of the nanoparticles changed by a factor of more than 10 depending on the tested cell culture [47].

The assessment of the potential gene knockdown activity of lipoplexes was performed by means of flow cytometry upon incubation of the lipid mixture with a siRNA able to downregulate the expression of GFP (siRNA$_{antiGFP}$) to form GCL/MOG-siRNA$_{antiGFP}$ lipoplexes at $\alpha = 0.7$ and $\rho_{eff} = 5$ and 10. Once lipoplexes were formed, these were incubated in the presence of human serum to form a protein corona (PC) on the nanovector surface in order to configure the real biological entity cells will see. Such PC-coated GCL/MOG-siRNA$_{antiGFP}$ lipoplexes were administered to HeLa-GFP and T731-GFP cells to analyse the potential induced GFP knockdown expression in these cells after 48 and 72 h post-administration. Flow cytometry data were collected in terms of mean fluorescence intensity, MFI (i.e., average intensity of fluorescence per cell) and expressed %GFP (percentage of cells in which GFP expression is observed). Free siRNA and Lipo2000*-siRNA$_{non\text{-}targeting}$ were used as negative controls, while Lipo2000*-siRNA$_{antiGFP}$ was the positive one.

As shown in Fig. 2, administration of free siRNA$_{antiGFP}$ (white bars) demonstrated the necessity of a vector-assisted delivery strategy to protect the silencing agent from nuclease degradation as a reduction of MFI after administration was not observed in GFP-overexpressing HeLa cells. Compared to untreated cells (green bars), we observed that the MFI signal decreased in HeLa-GFP at both lipoplex complexation conditions (ρ_{eff} = 5 and 10) after 48 and 72 h. This reduction was particularly pronounced at the shortest incubation time for the highest lipid content studied ($\rho_{eff} = 10$), and was rather higher than that observed for the Lipo2000*- siRNA$_{antiGFP}$ positive control. This points to a suitable internalization of the nanocarrier inside cells and subsequent cargo release in the cytoplasm (see below for details). However, additional administrations would be required to completely suppress GFP expression and compensate additional cell proliferation upon incubation [43,44]. It is also worth mentioning that the reduction of the MFI value (or %GFP one) was a consequence of the siRNA$_{antiGFP}$ sequence, since the cells treated with lipoplexes carrying a scrambled siRNA (pink bars) showed similar MFI or %GFP values as the untreated, healthy ones. Conversely, in T731-GFP cells MFI decrease was hardly detected after 48 h of incubation but present after 72 h, again particularly important at $\rho_{eff} = 10$ (see Fig. S2 of Supporting Information). It is worth mentioning that no changes in MFI were observed for the Lipo2000*-siRNA$_{antiGFP}$ control in the astrocyte cell line, which once highlights again the dependence of protein knockdown on cell phenotype and, thus, the need of development of personalized medicines to achieve optimal therapeutic outcomes in the desired target cell/tissue. Similar conclusions were reached when analysing the %GFP data (see Fig. S2), except for T731-GFP cells after 72 h of incubation at $\rho_{eff} = 5$, for which no fluorescent changes were observed. Overall, it seems that $\rho_{eff} = 10$ would be the optimum formulation for GCL/MOG-siRNA$_{antiGFP}$ lipoplexes to transfect siRNA into both HeLa-GFP and T731-GFP cell lines, which is in agreement with previous studies where amino-acid-based lipid nanocarriers based on lysine-derived monocationic lipid or histidine-derived gemini cationic lipid were used to transfect plasmid DNAs such as pCMV-Luc or pGFP [37,38,43,44].

Epifluorescence microscopy images were also acquired to evaluate the GFP knockdown expression by LNPs after 72 h of incubation in order to corroborate flow cytometry data. Fig. 3 show the fluorescence signal resulting from GFP expression in T731-GFP cells treated with GCL/MOG-siRNA$_{antiGFP}$ lipoplexes at $\alpha = 0.7$ and ρ_{eff} = 5 and 10 as examples. Lipo2000*-siRNA$_{antiGFP}$-treated and untreated T731-GFP cells were used as controls. Cell nuclei and cytoplasms were stained with DAPI (λ_{ex} = 350 nm) and Alexa Fluor 647 (λ_{ex} = 650 nm), respectively. Images were analyzed by ImageJ to quantify the mean fluorescence of cells (see Fig. S3) as explained in the Experimental Section. MFI values were observed to decrease upon administration of GCL/MOG-siRNA$_{antiGFP}$ lipoplexes a 55 % of the initial cell fluorescence signal intensity for ρ_{eff} = 5 and 74 % for ρ_{eff} = 10, respectively, whereas the values for the Lipo2000*-siRNA$_{antiGFP}$ control remained significantly much higher. Hence, the present observations agree with flow cytometry data discussed above; nonetheless, it is necessary to bear in mind that in spite of epifluorescence experiments makes use of a quantitative method of quantification they are affected by both illumination conditions, definition of ROIs and background substraction, and, therefore, they support but do not fully replace the results obtained by flow cytometry.

For an effective silencing therapy siRNA must be released inside the

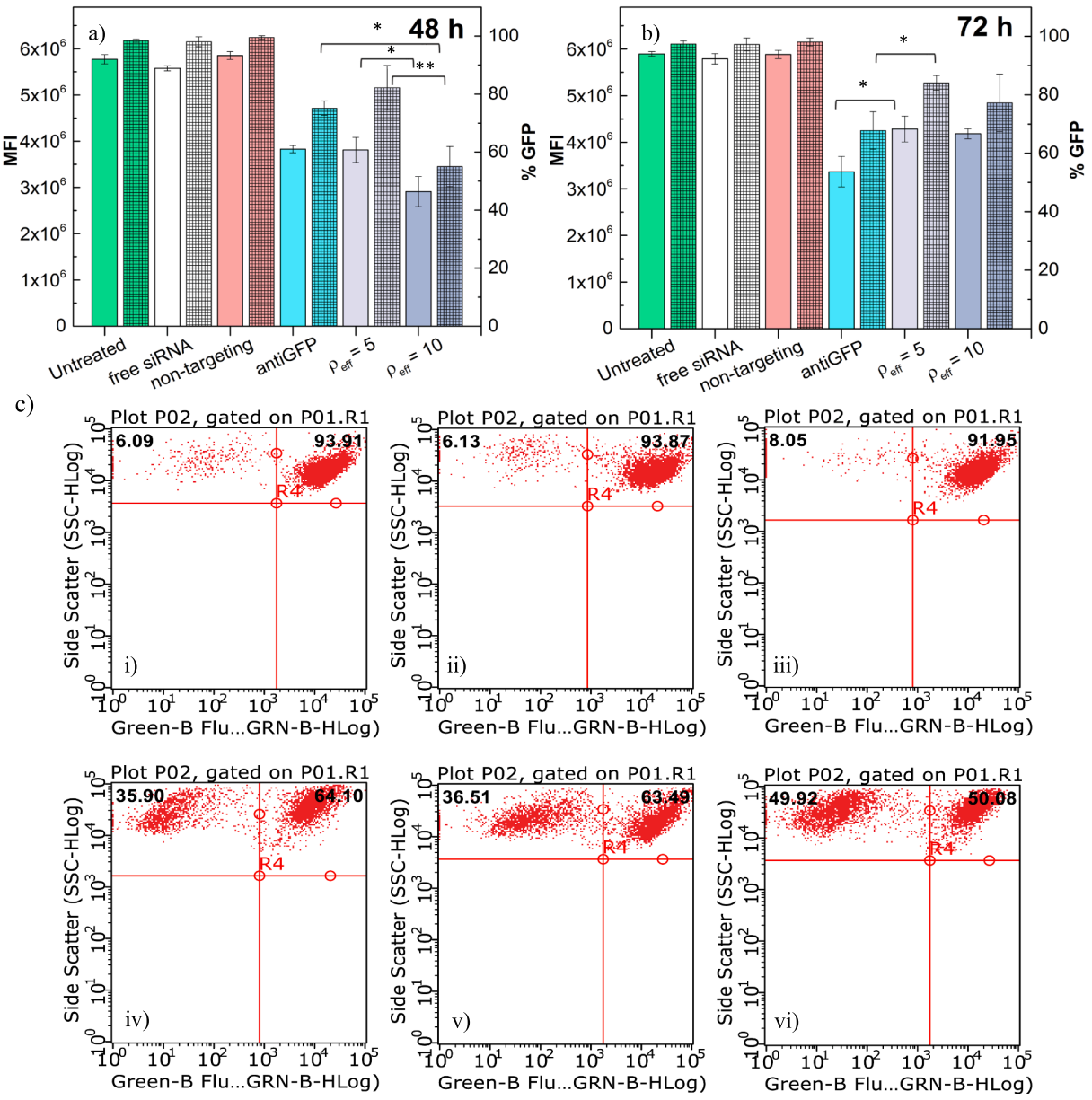

Fig. 2. GFP knockdown levels expressed as MFI (unshaded bars) and %GFP (shaded bars) in HeLa-GFP cells at 48 (a) and 72 h (b) of treatment obtained from flow cytometry data. Cells treated by GCL/MOG-siRNA$_{antiGFP}$ lipoplexes were collected at $\alpha = 0.7$ and $\rho_{eff} = 5$ (purple light bars) and 10 (purple dark bars). Untreated cells were used as a reference of the highest MFI and %GFP value (green bars). Free siRNA$_{antiGFP}$ and Lipo2000*-siRNA$_{non\text{-}targeting}$ were used as negative controls (white and pink bars, respectively) while Lipo2000*-siRNA$_{antiGFP}$ was used as positive control (blue bars). All experiments were performed with 10 % of HS. The data represent the mean ± SD of three independent wells. In the X-axis legend plots, untreated refers to bare cells; free siRNA to freely administered siRNA$_{antiGFP}$; non-targeting to Lipo2000*.siRNA$_{non\text{-}targeting}$ lipoplexes; antiGFP to Lipo2000*-siRNA$_{antiGFP}$ ones, and $\rho_{eff} = 5$ and $\rho_{eff} = 10$ to GCL/MOG-siRNA$_{antiGFP}$ lipoplexes at $\alpha = 0.7$ and $\rho_{eff} = 5$ and 10, respectively. *P < 0.05; **P < 0.01. Non-statistical differences are not indicated for major clarity. (c) Examples of scatter plots from flow cytometry data obtained after particle administration and subsequent incubation for 48 h: i) untreated cells; ii) free siRNA$_{antiGFP}$; iii) Lipo2000*-siRNA$_{non\text{-}targeting}$; iv) Lipo2000*-siRNA$_{antiGFP}$; v) GCL/MOG-siRNA$_{antiGFP}$ lipoplexes at $\rho_{eff} = 5$; and vi) GCL/MOG-siRNA$_{antiGFP}$ lipoplexes at $\rho_{eff} = 10$, respectively. The number inside the scatter plots represent de % cell population within the chosen threshold to distinguish cells between strongly fluorescent and weakly/non-fluorescent. (For interpretation of the references to colour in this figure legend, the reader is referred to the web version of this article.)

cell cytoplasm in optimal concentration playing, thus, the involved lipoplex internalization mechanisms a key role. In this regard, based on experimental observations endocytosis or endocytosis-like mechanisms have been proposed as the main pathways of internalization for lipoplexes rather than their fusion with plasma membrane [48]. To gain further knowledge about the predominant internalization pathway, if any, of the present GCL-based lipoplexes, HeLa-GFP and T731-GFP cells were treated prior lipoplex administration with known biochemical inhibitors of energy-dependent, clathrin-mediated and caveolae-mediated endocytosis as well as of micro- and macropinocytosis (see Fig. 4 and Experimental Section for details).

To investigate the energy dependent-based mechanism, cells were preincubated in the presence of NaN_3/2-deoxyglucose (NaN_3/DOG) and then, treated with the lipoplexes. NaN_3/DOG, which blocks cellular ATP synthesis, resulted in decreases of nanocarrier cellular internalization of ca. 37 and 22 % for HeLa-GFP and T731-GFP cells, respectively, indicating that non-specific endocytosis plays a relatively important role in lipoplex uptake. Larger inhibitions were not observed most likely because of the presence of exogenous ATP and glucose in the cell culture medium. To discern any role that caveolae-mediated endocytosis may

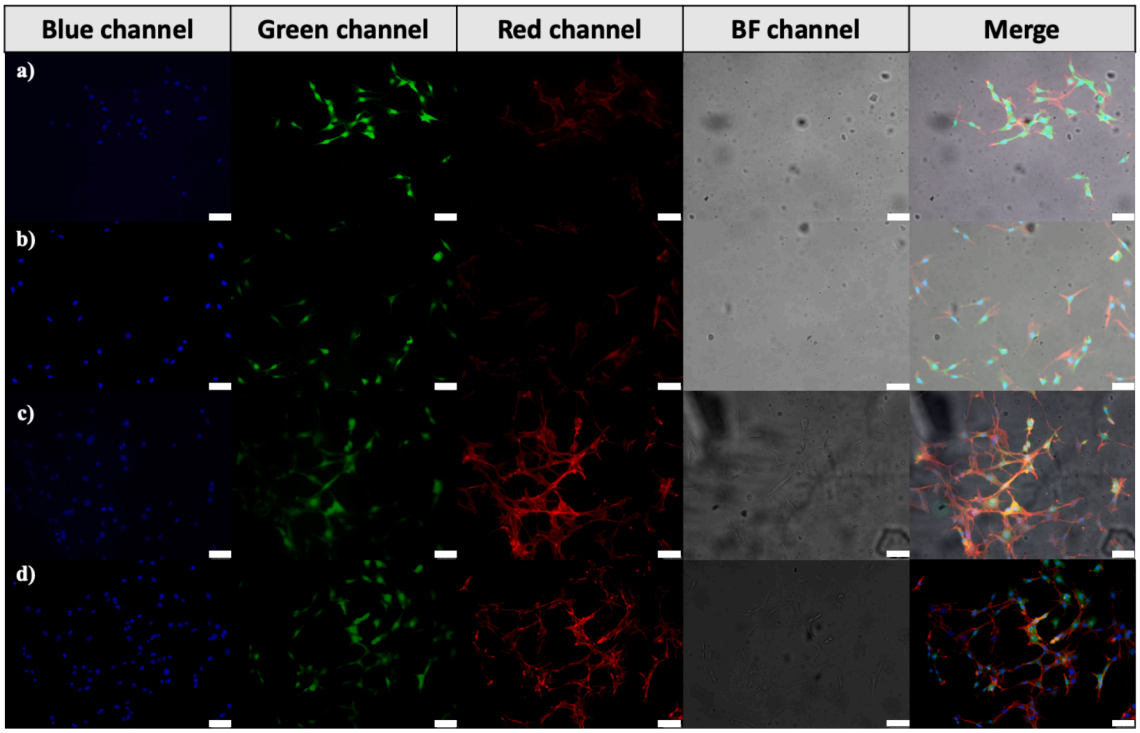

Fig. 3. Epifluorescence microscopy images of T731-GFP cells treated with GCL/MOG-siRNA$_{antiGFP}$ lipoplexes at $\alpha = 0.7$ and $\rho_{eff} = 5$ (row c) and 10 (row d) in the presence 10 % HS) after 72 h of incubation. Untreated cells (row a) and cells treated with Lipo2000*siRNA$_{antiGFP}$ (row b) were used as controls. The green channel shows the GFP fluorescence intensity, the blue one the fluorescence from cell nucleus stained with DAPI ($\lambda_{ex} = 350$ nm), the red one the Alexa Fluor 647 ($\lambda_{ex} = 650$ nm) fluorescence signal from cell cytoplasm, the BF channel shows the images on bright field, and the merged images represent the combination of all previous channels. Scale bars are 75 μm. (For interpretation of the references to colour in this figure legend, the reader is referred to the web version of this article.)

play in lipoplex uptake, two inhibitors were used: genistein, a tyrosine kinase inhibitor which prevents both actin depolymerization in the local cortical cytoskeleton, which must precede internalization of caveolar vesicles, and recruitment of dynamin 2 required for the scission of vesicles from cell membrane [49]; and methyl-β-cyclodextrin, a cyclic heptasaccharide known to sequester and alter cholesterol-rich domains within the plasma membrane, involved in raft lipid formation [50]. For both drugs, inhibition of nanoparticle internalization was hardly detected, which confirms that caveolae-mediated endocytosis as well as lipid-raft-mediated uptake are not directly involved in lipoplex entry inside both cell lines. This behaviour may be related to the size of the present particles since, for example, caveolae generally can only endocytose nanoparticles in the range of 50–100 nm [51], whereas our lipoplexes have an average hydrodynamic diameter of (240 ± 30) nm (see Fig. S4 in Supporting Information), clearly above the size of the mixed GCL/MOG liposomes (157 ± 15) nm (dotted line in the graph). Moreover, an average PDI value of (0.25 ± 0.06) make them suitable (PDI < 0.3) as nucleic acid nanovectors, as previously reported in literature [52,53]. Similar results were observed for the internalization of GCL/MOG-siRNA$_{antiGFP}$ lipoplexes in the presence of cytochalasin D, which inhibits macropinocytosis through the depolymerization of actin filaments and tubulin microtubules [54]. A very slight inhibition of particle internalization promoted by this compound was detected (ca. 12 %), which would agree with the fact that both HeLa-GFP and T731-GFP are non-phagocytosing cells. Moreover, to decipher the role of clathrin-mediated endocytosis two other specific drug inhibitors were used, the dynamin-GTPase inhibitor dynasore, required for budding of clathrin-coated vesicles from the plasma membrane, and the cationic amphipathic drug chlorpromazine, which anchors clathrin and adaptor protein 2 (AP2) complex to endosomes, thereby preventing the assembly of coated pits at the inner surface of the plasma membrane [55]. Flow cytometry data showed that dynasore administration to cells led to a decrease in lipoplex uptake of ca. 27 % in HeLa-GFP whereas only 9 % for T731-GFP. Conversely, although chlorpromazine reduced lipoplex internalization in HeLa cells ca. 41 %, the decrease was much more significant in T731-GFP ones, ca. 61 % of the nanoparticles compared to controls. Because of the amphipathic nature of chlorpromazine, this drug is readily capable of incorporating into the lipid bilayer of the plasma membrane increasing lipid fluidity which, in turn, may hinder or inhibit the formation of membrane invaginations, which results in the present case in a decrease in particle internalization [50]. These data, then, should confirm the predominant role of the clathrin-mediated pathway for lipoplex internalization, and reinforce the idea that the specific roles played by different mechanisms in lipoplex uptake may, at least in part, depend on the cell type (Fig. 4) [56].

In summary, all these experiments strongly suggest that clathrin-mediated and, to a lesser extent, energy dependent endocytosis are involved in the lipoplex internalization process, but the lack of specific drugs leading to >80 % inhibition of internalization may point to the role played by some other alternative, not targeted routes for endocytosis, as, for example, poorly characterized clathrin- and caveolae-independent, non-macropinocytic pathways [57], the simultaneous use of several mechanisms for successful particles internalization, and/or the presence of cross-talk mechanisms between endocytic pathways, that is, the alteration of one pathway might modulate another for compensation [58]. For example, it cannot be completely disregarded that a small proportion of GCL/MOG-siRNA$_{antiGFP}$ lipoplexes would directly cross the plasma membrane establishing suitable interactions [59], as occurred for other types of lipoplexes containing, for example, DOTAP, DOTMA, DOPE and cardiolipin (CL) [60], and considering that MOG helper lipid here used is known to fluidize and stabilize the lipidic structures, but can also collaborate in the formation of lipidic phases able to enhance fusogenicity, thus, contributing to a higher transfection efficiency [19]. In addition, it is worth mentioning that the PC adsorbed onto the lipoplexes may also play a favorable role to enhance the internalization process by either inducing binding to specific cell surface

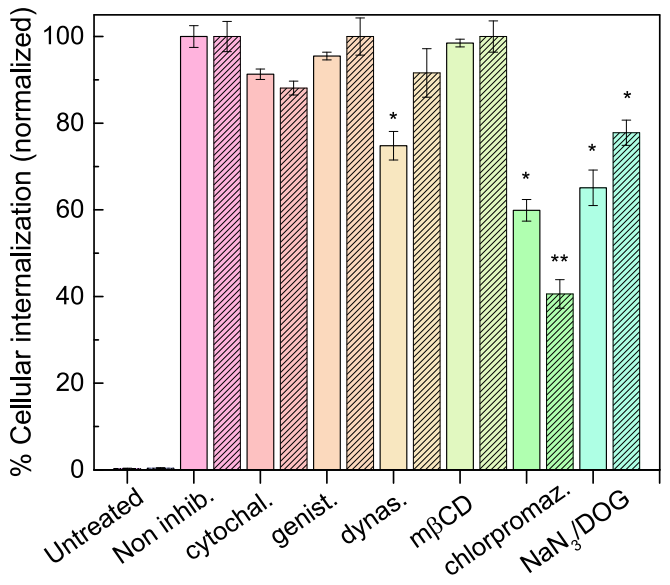

Fig. 4. Normalized cellular internalization analyzed by flow cytometry after the administration of GCL/MOG-siRNA$_{antiGFP}$ lipoplexes at $\alpha = 0.7$ and $\rho_{eff} = 10$ to HeLa-GFP (unstripped columns) and T731-GFP (stripped columns) cells in the presence of different inhibitors of specific internalization pathways: cytochalasin, genistein, dynasore, methyl-β-cyclodextrin, chlorpromazine and sodium azide/2-deoxyglucose. Percent of internalization was normalized to particle internalization in the absence of inhibitors. Untreated cells with lipoplexes and inhibitors were used as negative control. Statistical significance compared to non-inhibited cells at each group: * = $P < 0.05$; ** = $P < 0.01$. In X-axis labels, Untreated refers to incubation of bare cells without added lipoplexes, whereas Non inhib. refers to cells receiving the lipoplexes without the addition of any inhibitor compound. The remaining labels correspond to the abbreviation of each of the inhibitors added to cell cultures.

receptors [61] and/or by modifying the lipoplex conformation [62], which would help to explain the incomplete observed inhibitions.

In this regard, to confirm the structure and conformation of the present lipoplexes in the presence of the PC, SAXS experiments were performed at $\alpha = 0.7$ and $\rho_{eff} = 5$ and 10, in the absence and presence of HS, as shown in Fig. 5a. First, in the absence of HS, that is, when no PC is formed onto the lipoplexes, the diffractograms show Bragg peaks with Miller indices (*h k l*) compatible with two coexisting L_α lamellar structures, $L_{\alpha,1}$ (black) and $L_{\alpha,2}$ (green), possibly due to the presence of two different multilamellar domains within GCL/MOG-siRNA lipoplexes with very close but distinguishable interlamellar distances (see Table S1 in the Supporting Information, that collects *d* values calculated directly from *q* factors related to (1 0 0) peak as ($d = 2\pi/q_{100}$)). The L_α structure is a multilamellar lyotropic liquid crystal phase, characterized by a stacking of mixed lipid bilayers, where siRNA helixes may be allocated, compacted, and protected in the aqueous layer between each pair of lipid bilayers in a sandwhich-like fashion (see left of Fig. 5b). This structure is typically found in GCL/DOPE-pDNA lipoplexes [14,26,27,29,34,37,38], and also in GCL/MOG-siRNA lipoplexes with low MOG content (i.e., moderate-to-high α values as in the present study) [33,44].

The above-mentioned L_α phases ($L_{\alpha,1}$ and $L_{\alpha,2}$) also appears in the presence of the PC surrounding the lipoplex surface (with almost no variation in *d*, see Table S1); however, it is striking to note the appearance of a series of peaks at low *q* values with the same pattern at both ρ_{eff} = 5 and 10. A detailed analysis of the diffractograms reveals that these peaks are due to three additional L_α phases coming from the two main L_α phases (see *hkl* assignment on the diffractograms of Fig. 5a), with interlamellar distances larger than those of the starting structures. This evidence, also found in other DNA- or siRNA-lipoplexes [43,44,63], might be indicating that the presence of proteins on the lipoplex surface induces a slight decompaction of the lipid bilayer stacking (i.e., the interlamellar distance, d, increases, see right of Fig. 5b), to a different extent depending on whether the starting structure is $L_{\alpha,1}$ or $L_{\alpha,2}$. Obviously, this implies that both the thickness of the bilayer (d_m) and the thickness of the aqueous layer (d_w) will be affected, since $d = d_m + d_w$. In fact, $L_{\alpha,1}$ splits into two L_α phases: $L_{\alpha,1}$ (black) and $L_{\alpha,1}'$ (pink), while $L_{\alpha,2}$ splits into three L_α phases: $L_{\alpha,2}$ (green), $L_{\alpha,2}'$ (red) and $L_{\alpha,2}''$ (blue). If $L_{\alpha1}$ (black) is compared with $L_{\alpha,1}'$ (pink), the structure expands by around 55 % on average. On the other hand, if $L_{\alpha,2}$ (green) is compared with $L_{\alpha,2}'$ (red) and $L_{\alpha,2}''$ (blue), the structure expands by 33 % and 11 %, respectively, with respect to the original starting structures (without PC). Note how the peak intensity (area under the peak) of the main L_α phases decrease in favor of the additional peaks appearing in the L_α phases found in the presence of PC. Previous reports have demonstrated that the coexistence of different lyotropic liquid crystal phases, as those found in the present work, may enhance transfection or silencing efficiencies [64,65], particularly in the presence of HS [26,27,29,33,34,43,44,63,66–68] and can be considered a potential and interesting beneficial effect. Thus, our present data would agree with an additional contribution to cellular uptake by an alternative, non-blocked pathway, at least to high extents, by any of the inhibitors here used [48,69].

It is well-known that reaching the biological targets and ensuring sufficient drug delivery and accumulation is extremely challenging as consequence of the multiple biological barriers that characterize tumors and their complex microenvironment, which then may largely limit the efficacy of currently developed nanomedicines [24]. Despite their relative ease of handling, 2D cultures do not show any structural architecture and lack the complex physiology and organization of real tumor tissues, as well as they do not replicate either (*i*) the cell-to-cell and cell-to-extracellular matrix (EMC) interactions, and (*ii*) the oxygen, nutrients, and pH gradients which play a crucial role in tumor progression, chemoresistance and metastatic spread [70–72]. For such reasons, 3D HeLa-GFP and T731-GFP tumor spheroids were grown in order to analyse under more physiologically-relevant conditions the ability of GCL/MOG-siRNA$_{antiGFP}$ lipoplexes to penetrate the tumoral microenvironment and inside tumour cells and release their siRNA cargo to exert the GFP down-regulation activity. Fig. S5 shows the size and morphological temporal evolution of both 3D HeLa-GFP and T731-GFP tumour spheroids. It can be observed that both cell lines (row (a) in both figures, untreated cells) can give rise to well-supported tumoral spheroids that progressively grow with time until reaching sizes of ca. 1.5 ± 0.4 and 0.6 ± 0.2 μm for HeLa-GFP and T731-GFP cells, respectively, as observed from confocal microscopy images. Also, it is worth mentioning that T731-GFP spheroids showed a very compact core surrounded by a layer of more loosely attached cells; conversely HeLa-GFP ones have a more regular, perfectly defined spherical morphology.

Next, GCL/MOG-siRNA$_{antiGFP}$ lipoplexes doped with Nile Red (200:1 lipid:fluorescent probe molar ratio, see Experimental Section for details) were injected to the cell culture medium surrounding the spheroids. Here, Nile Red was chosen as the fluorescent probe since: *i)* this dye is a polarity-sensitive fluorescent probe for intracellular lipids and protein hydrophobic domains, with tunable fluorescence signal from golden yellow to deep red depending on the lipid environment [73]; *ii*) its fluorescent signal in polar media is very weak; *iii*) it is poorly soluble in aqueous solution; and *iv*) it is also commonly used as a hydrophobic drug model in release studies [74]. Thus, the ability of lipoplex nanocarriers to penetrate the tumoral spheroid was monitored by means of the increasing red fluorescence signal of the Nile Red dye when residing in an apolar microenvironment (the lipid multilamellar structure) as well as by the reduction of cellular GFP fluorescence thanks to the effective release of the siRNA cargo loaded inside the lipoplexes into cells, respectively. Fig. 6 and Fig. S6 show that there is hardly penetration of the lipoplexes inside the spheroids after 1 h of incubation, as determined by a scarce 4 and 6 % of Nile red fluorescent intensity enhancement for HeLa and T731 cells, respectively. In particular, for HeLa 3D culture

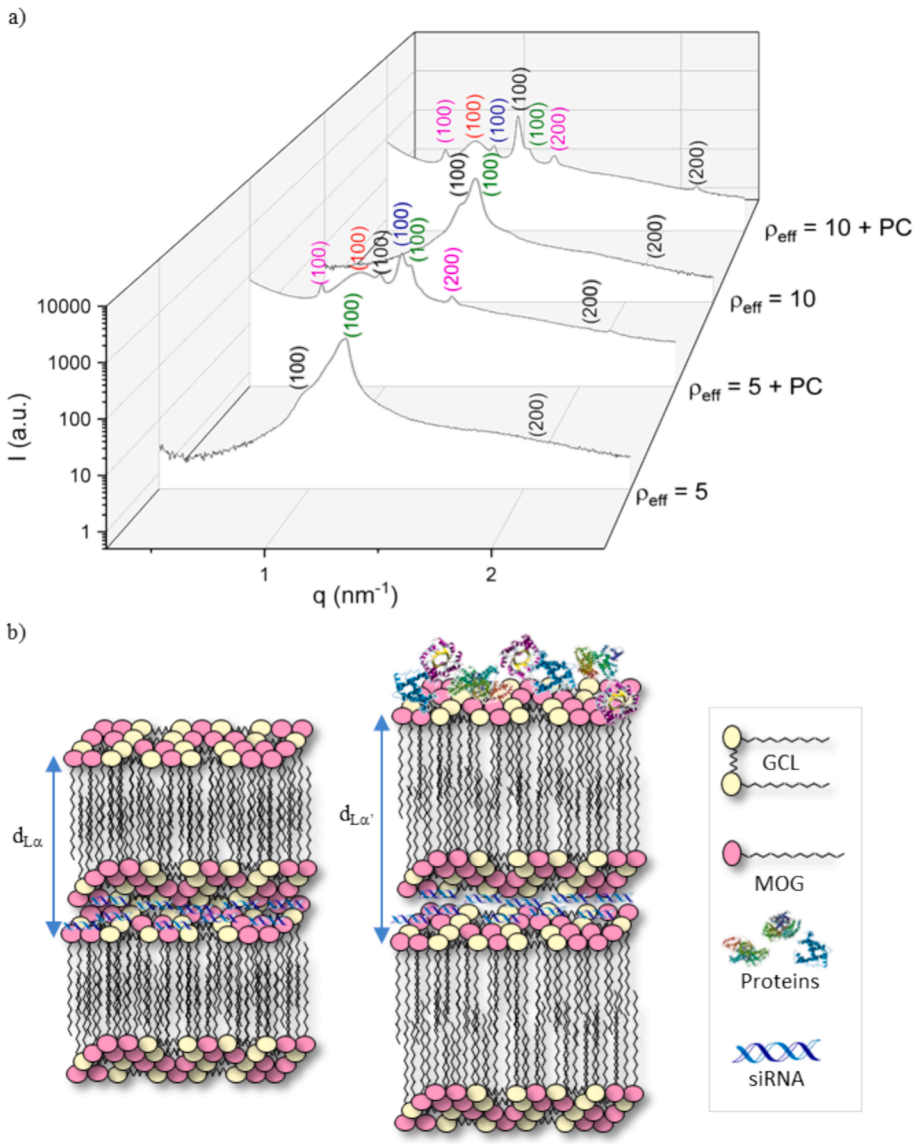

Fig. 5. (a) SAXS diffractograms of GCL/MOG-siRNA lipoplexes at α = 0.7, and ρ_{eff} = 5 and 10, in the absence and presence of PC. (b) Schematic drawing of L_α multilamellar phase, in absence (left) and presence of PC (right).

only some few red dots can be distinguished while remaining red fluorescence signal is perimetrically detected around the spheroids without turning off the GFP fluorescence (Fig. 6). A similar observation was made for T731-GFP spheroids, in which the Nile Red fluorescence is not only observed surrounding the cell spheroid but also on its surface. Such observed difference may arise from the smaller size of T731-GFP spheroids compared to HeLa-GFP ones. Moreover, the decrease in GFP intensity for HeLa spheroids is negligible, whereas for T731-GFP is of ca. 23 % of the initial intensity of non-treated astrocytes spheroids, respectively.

After incubation for 24 h, the observed situation is rather different. For both types of spheroids, Nile Red fluorescence can be observed largely distributed along the spheroids (Fig. 6 and Fig. S6) being particularly more intense in HeLa cells, with a 69 % of red fluorescence enhancement compared to only the 31 % for T731 cell, respectively. This difference may point to a certain penetration of the lipoplexes inside the spheroid structure followed by cell uptake and subsequent, at least partially, cargo release of the fluorescent probe inside cells. Such uptake inside spheroid-contained cells is also corroborated by a certain decrease in the green fluorescence of those cells mainly located at the middle, surface plane of the spheroid, which also displays the highest intensity of Nile Red (white circles in Fig. 6). Specifically, a decrease in mean GFP fluorescent signal intensity of ca. 58 % and 40 % of the initial fluorescence after treatment is observed for both HeLa and T731 cells (see Fig. S7a-b), respectively, which is significantly larger than that observed for non-treated spheroids. In the latter case, the observed GFP signal intensity reduction of ca. 43 and 28 % of the initial GFP fluorescence signal for HeLa and T731 cells, respectively, can be a consequence of the progressive death of cells located at the inner, hypoxic spheroid core.

After further incubation up to 96 h, the natural fluorescence of non-treated HeLa-GFP and T731-GFP spheroids undergoes an additional reduction of up to ca. 73 % and 49 % of the initial detected green fluorescence signals, respectively (see Fig. S7a–b), which can be related to additional cell death in the spheroid core, as mentioned above. But such reduction is much more intense in cell spheroids treated with the siRNA-loaded lipoplexes, with GFP fluorescence intensity reductions of up to 89 and 76 % of the initial values for both HeLa-GFP and T731 cell spheroids, respectively, thus, indicating that protein down-regulation can be effectively achieved for both types of cells. It is also worth mentioning that the protein signal depletion in T731-GFP 3D tumoral spheroids takes mainly place at the external area, being the core still

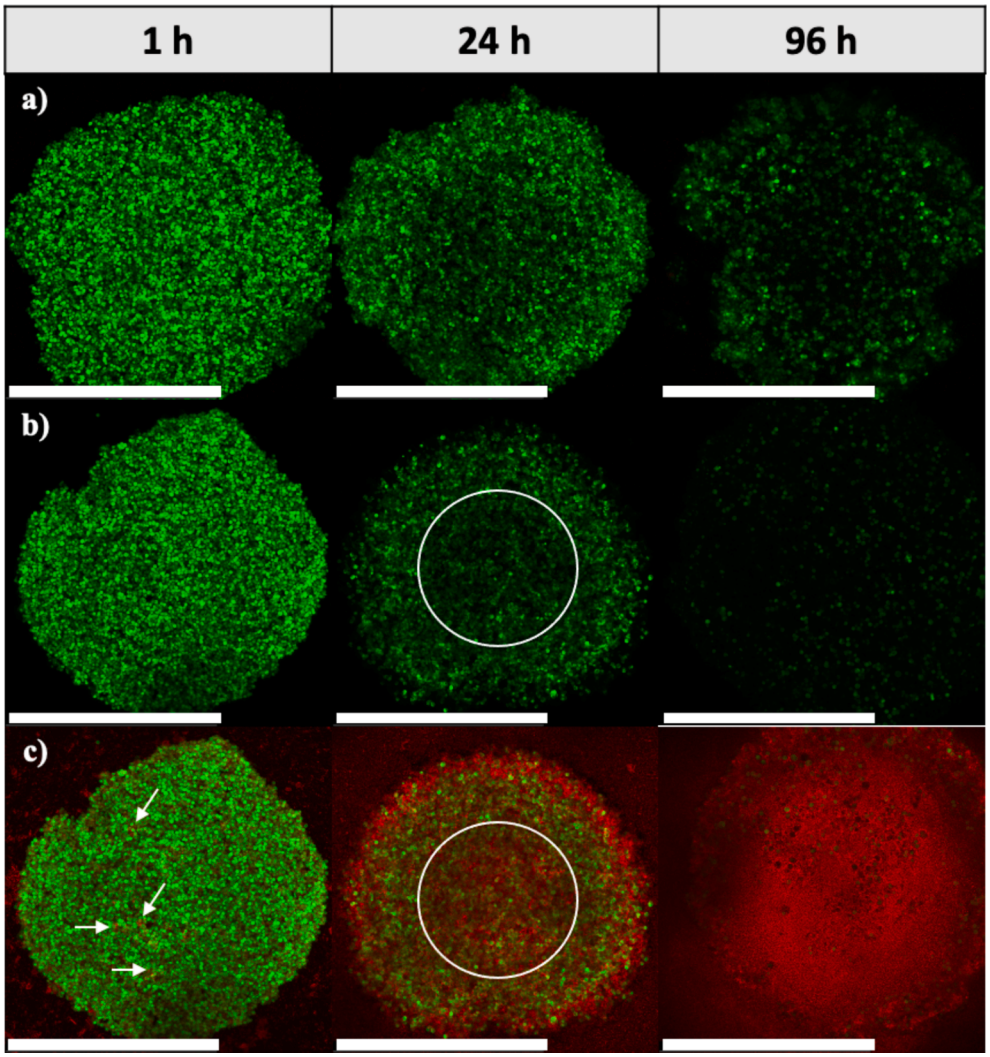

Fig. 6. Confocal microscopy images of HeLa-GFP spheroids treated with GCL/MOG-siRNA$_{antiGFP}$ lipoplexes at $\alpha = 0.7$ and $\rho_{eff} = 10$ (rows b and c) in the presence 10 % HS after different incubation times. Untreated cells (row a) were used as controls. Row b) shows the green channel with GFP fluorescence intensity, whereas row c) displays the overlay of GFP and Nile Red fluorescence signals. The white circles indicate the core area of the spheroids. Scale bars are 1 mm. (For interpretation of the references to colour in this figure legend, the reader is referred to the web version of this article.)

fluorescent. Such observations might be related to a relatively more compact spheroid formed by these brain cells and/or a lower ability of lipoplexes to be uptaken by this astrocyte cell line. On the other hand, the former observations are further corroborated by the observed enhancements of the Nile Red fluorescent signals inside the cell spheroids, which are rather enhanced reaching values of ca. 98 and 47 %, respectively.

Hence, the present lipoplexes with protein coating configure a biological entity able to penetrate inside the complex tumoral microenvironment to transport siRNA efficiently and provide a successful release of its cargo inside the target cells, thus, achieving an effective inhibition of GFP protein expression herein as proof of concept, which further corroborates the results previously obtained using simpler 2D cultures. Therefore, this kind of LNP bearing a GCL as main component opens new avenues for the development of non-toxic, effective nanomedicines for silencing gene therapy not only for cancer, but also for other diseases such as cardiovascular or neurodegenerative ones.

4. Conclusions

The LNP constituted by a gemini cationic lipid with quaternary ammonium cationic head groups and the neutral mono oleoyl glycerol proved biocompatible and safe in the cells studied. No relevant levels of ROS or cytotoxicity were detected. In fact, they were better than those found for the commercial control used Lipo2000* in some cases. The physical and structural studies performed with agarose gel electrophoresis, DLS, SAXS and ζ-potential techniques corroborated the siRNA incorporation in a lamellar pattern (L_α) with sizes around 240 nm and charge of ca. +25 mV. The *in vitro* experiments were always carried out on cells from different tumours to see the diverse biological responses and analysed by flow cytometry and epifluorescence or confocal microscopy. The major reduction of the MFI value (or %GFP) was noted at $\rho_{eff} = 10$ in both cells. However, in the case of HeLa-GFP cells, the gene knockdown was more noticeable after 48 h of incubation while for T731-GFP cells was at 72 h. The nanovector internalization mechanism inside the cells seemed to be mainly dominated by a clathrin-mediated pathway. However, it must be considered that the PC may also play a crucial role in the cellular uptake: the PC can modify the nanovector structure as seen from the slight decompaction of the lipid bilayer stacking in the SAXS experiments here reported. Finally, encouraging results were observed from 3D spheroids cell cultures, since after 24 h of incubation penetration of the nanovector and cellular uptake (GFP knockdown) inside tumour spheroids were observed. The reduction of the GFP signal in the spheroids was more significant for human cervical

cancer cells than for mouse astrocyte cancer cells. And this gene knockdown was distinguished in different areas of the spheroid, possibly due to the clear differences in size and thus, compactness between the tumour aggregates. This study helps to put a spotlight on these types of nanovectors for clinical applications, corroborating the importance of designing specific or personalized strategies depending on the disease, tissue, organ, and/or environment under study. Further studies in 2D and 3D-grown cells will be required to explore in depth the cellular uptake pathways, the protein corona effect surrounding the nanovector, and how the GFP expression behaves over time after additional/sequential administrations.

CRediT authorship contribution statement

Natalia Sánchez-Arribas: Visualization, Validation, Methodology, Investigation. **Brenda Velasco Rodríguez:** Validation, Resources, Investigation. **Emilio Aicart:** Writing – review & editing, Methodology, Formal analysis, Data curation, Conceptualization. **Andrés Guerrero-Martínez:** Writing – review & editing, Visualization, Funding acquisition, Formal analysis, Data curation. **Elena Junquera:** Writing – review & editing, Writing – original draft, Supervision, Project administration, Funding acquisition, Conceptualization. **Pablo Taboada:** Writing – review & editing, Writing – original draft, Supervision, Project administration, Funding acquisition, Conceptualization.

Declaration of competing interest

The authors declare that they have no known competing financial interests or personal relationships that could have appeared to influence the work reported in this paper.

Acknowledgements

P.T. thanks Agencia Estatal de Investigación (AEI) for funding through project PID2022-142682OB-I00 and PCI2022-134981-2, and Xunta de Galicia for grant ED431C 2022/28. ERDF funds are also acknowledged; **E.J. thanks** Agencia Estatal de Investigación (AEI) for funding through project PID2021-123228NB-I00.

Appendix A. Supplementary material

Supplementary data to this article can be found online at https://doi.org/10.1016/j.jcis.2024.10.115.

Data availability

Data will be made available on request.

References

[1] L.D. Kong, J.R. Qiu, W.J. Sun, J. Yang, M.W. Shen, L. Wang, X.Y. Shi, Multifunctional PEI-entrapped gold nanoparticles enable efficient delivery of therapeutic siRNA into glioblastoma cells, Biomater. Sci. 5 (2017) 258–266.
[2] C.E. Dunbar, K.A. High, J.K. Joung, D.B. Kohn, K. Ozawa, M. Sadelain, Gene therapy comes of age, Science 359 (2018) eaan4672.
[3] F. Liu, C.F. Wang, Y.T. Gao, X. Li, F. Tian, Y.T. Zhang, M.Y. Fu, P.F. Li, Y.L. Wang, F. Wang, Current transport systems and clinical applications for small interfering RNA (siRNA) drugs, Mol. Diagn. Ther. 22 (2018) 551–569.
[4] R.C.C. Ryther, A.S. Flynt, J.A. Phillips, J.G. Patton, siRNA therapeutics: big potential from small RNAs, Gene Ther. 12 (2005) 5–11.
[5] H. Chang, J. Zhang, H. Wang, J. Lv, Y.Y. Cheng, A combination of guanidyl and phenyl groups on a dendrimer enables efficient siRNA and DNA delivery, Biomacromolecules 18 (2017) 2371–2378.
[6] M. Foldvari, D.W. Chen, N. Nafissi, D. Calderon, L. Narsineni, A. Rafiee, Non-viral gene therapy: gains and challenges of non-invasive administration methods, J. Control. Release 240 (2016) 165–190.
[7] E. Villar-Alvarez, B.H. Leal, A. Cambon, A. Pardo, R. Martinez-Gonzalez, J. Fernandez-Vega, S. Al-Qadi, V.X. Mosquera, A. Bouzas, S. Barbosa, P. Taboada, Triggered RNAi therapy using metal inorganic nanovectors, Mol. Pharm. 16 (2019) 3374–3385.
[8] E. Villar-Alvarez, B.H. Leal, R. Martinez-Gonzalez, A. Pardo, S. Al-Qadi, J. Juarez, M.A. Valdez, A. Cambon, S. Barbosa, P. Taboada, siRNA silencing by chemically modified biopolymeric nanovectors, ACS Omega 4 (2019) 3904–3921.
[9] N. Bono, F. Ponti, D. Mantovani, G. Candiani, Non-viral in vitro gene delivery: it is now time to set the bar!, Pharmaceutics 12 (2020) 23.
[10] A.J. Mellott, M.L. Forrest, M.S. Detamore, Physical non-viral gene delivery methods for tissue engineering, Ann. Biomed. Eng. 41 (2013) 446–468.
[11] P.R. Cullis, M.J. Hope, Lipid nanoparticle systems for enabling gene therapies, Mol. Ther. 25 (2017) 1467–1475.
[12] T. Ahmed, A.O. Kamel, S.D. Wettig, Interactions between DNA and Gemini surfactant: impact on gene therapy: part I, Nanomedicine 11 (2016) 289–306.
[13] T. Ahmed, A.O. Kamel, S.D. Wettig, Interactions between DNA and Gemini surfactant: impact on gene therapy: part II, Nanomedicine 11 (2016) 403–420.
[14] N. Sánchez-Arribas, M. Martínez-Negro, C. Aicart-Ramos, C.T. de Ilarduya, E. Aicart, A. Guerrero-Martínez, E. Junquera, Gemini cationic lipid-type nanovectors suitable for the transfection of therapeutic plasmid DNA encoding for pro-inflammatory cytokine interleukin-12, Pharmaceutics 13 (2021) 729.
[15] V. Perri, M. Pellegrino, F. Ceccacci, A. Scipioni, S. Petrini, E. Gianchecchi, A. Lo Russo, S. De Santis, G. Mancini, A. Fierabracci, Use of short interfering RNA delivered by cationic liposomes to enable efficient down-regulation of PTPN22 gene in human T lymphocytes, PLoS One 12 (2017) e0175784.
[16] S. Falsini, S. Ristori, L. Ciani, E. Di Cola, C.T. Supuran, A. Arcangeli, M. In, Time resolved SAXS to study the complexation of siRNA with cationic micelles of divalent surfactants, Soft Matter 10 (2014) 2226–2233.
[17] R.Q. Cruz, C.M. Morais, A.M. Cardoso, S.G. Silva, M.L. Vale, E.F. Marques, M. C. Pedroso de Lima, A.S. Jurado, Enhancing glioblastoma cell sensitivity to chemotherapeutics: a strategy involving survivin gene silencing mediated by Gemini surfactant-based complexes, Eur. J. Pharm. Biopharm. 104 (2016) 7–18.
[18] Z. Pietralik, Ż. Kołodziejska, M. Weiss, M.J.P.O. Kozak, Gemini surfactants based on bis-imidazolium alkoxy derivatives as effective agents for delivery of nucleic acids: a structural and spectroscopic study, PLoS One 10 (2015) e0144373.
[19] C. Costa, I.S. Oliveira, J.P.N. Silva, S.G. Silva, C. Botelho, M.L.C. do Vale, M.E.C. D. Real Oliveira, A.C. Gomes, E.F. Marques, Effective cytocompatible nanovectors based on serine-derived Gemini surfactants and monoolein for small interfering RNA delivery, J. Colloid Interface Sci. 584 (2021) 34–44.
[20] A. Wittrup, A. Ai, X. Liu, P. Hamar, R. Trifonova, K. Charisse, M. Manoharan, T. Kirchhausen, J. Lieberman, Visualizing lipid-formulated siRNA release from endosomes and target gene knockdown, Nat. Biotechnol. 33 (2015) 870.
[21] T.-M. Achilli, J. Meyer, J.R. Morgan, Advances in the formation, use and understanding of multi-cellular spheroids, Expert Opin. Biol. Ther. 12 (2012) 1347–1360.
[22] E.C. Costa, D. de Melo-Diogo, A.F. Moreira, M.P. Carvalho, I.J. Correia, Spheroids formation on non-adhesive surfaces by liquid overlay technique: considerations and practical approaches, Biotechnol. J. (2018) 13.
[23] S.M. Roy, V. Garg, S. Barman, C. Ghosh, A.R. Maity, S.K. Ghosh, Kinetics of nanomedicine in tumor spheroid as an in vitro model system for efficient tumor-targeted drug delivery with insights from mathematical models, Front. Bioeng. Biotechnol. 9 (2021) 785937.
[24] F. Hirschhaeuser, H. Menne, C. Dittfeld, J. West, W. Mueller-Klieser, L.A. Kunz-Schughart, Multicellular tumor spheroids: an underestimated tool is catching up again, J. Biotechnol. 148 (2010) 3–15.
[25] M.S. Oliveira, B. Aryasomayajula, B. Pattni, S.V. Mussi, L.A. Ferreira, V. P. Torchilin, Solid lipid nanoparticles co-loaded with doxorubicin and α-tocopherol succinate are effective against drug-resistant cancer cells in monolayer and 3-D spheroid cancer cell models, Int. J. Pharm. 512 (2016) 292–300.
[26] K. Kumar, A.L. Barrán-Berdón, S. Datta, M. Muñoz-Úbeda, C. Aicart-Ramos, P. Kondaiah, E. Junquera, S. Bhattacharya, E. Aicart, A delocalizable cationic headgroup together with an oligo-oxyethylene spacer in Gemini cationic lipids improves their biological activity as vectors of plasmid DNA, J. Mat. Chem. B 3 (2015) 1495–1506.
[27] A.L. Barrán-Berdón, S.K. Misra, S. Datta, M. Muñoz-Úbeda, P. Kondaiah, E. Junquera, S. Bhattacharya, E. Aicart, Cationic Gemini lipids containing polyoxyethylene spacers as improved transfecting agents of plasmid DNA in cancer cells, J. Mat. Chem. B 2 (2014) 4640–4652.
[28] M. Seoane, P. Iglesias, T. Gonzalez, F. Dominguez, M. Fraga, C. Aliste, J. Forteza, J. A. Costoya, Retinoblastoma loss modulates DNA damage response favoring tumor progression, PLoS One 3 (2008) e3632.
[29] S.K. Misra, M. Muñoz-Úbeda, S. Datta, A.L. Barrán-Berdón, C. Aicart-Ramos, P. Castro-Hartmann, P. Kondaiah, E. Junquera, S. Bhattacharya, E. Aicart, Effects of a delocalizable cation on the headgroup of Gemini lipids on the lipoplex-type nano-aggregates directly formed from plasmid DNA, Biomacromolecules 14 (2013) 3951–3963.
[30] K. Kantner, J. Rejman, K.V.L. Kraft, M.G. Soliman, M.V. Zyuzin, A. Escudero, P. del Pino, W.J. Parak, Laterally and temporally controlled intracellular staining by light-triggered release of encapsulated fluorescent markers, Chem. Eur. J. 24 (2018) 2098–2102.
[31] R. Lama, L. Zhang, J.M. Naim, J. Williams, A. Zhou, B. Su, Development, validation and pilot screening of an in vitro multi-cellular three-dimensional cancer spheroid assay for anti-cancer drug testing, Bioorg. Med. Chem. 21 (2013) 922–931.
[32] J. Gilleron, W. Querbes, A. Zeigerer, A. Borodovsky, G. Marsico, U. Schubert, K. Manygoats, S. Seifert, C. Andree, M. Stoter, H. Epstein-Barash, L.G. Zhang, V. Koteliansky, K. Fitzgerald, E. Fava, M. Bickle, Y. Kalaidzidis, A. Akinc, M. Maier, M. Zerial, Image-based analysis of lipid nanoparticle-mediated siRNA delivery, intracellular trafficking and endosomal escape, Nat. Biotechnol. 31 (2013) 638–U102.

[33] M. Martínez-Negro, K. Kumar, A.L. Barrán-Berdón, S. Datta, P. Kondaiah, E. Junquera, S. Bhattacharya, E. Aicart, Efficient cellular knockdown mediated by siRNA nanovectors of Gemini cationic lipids having delocalizable headgroups and oligo-oxyethylene spacers, ACS Appl. Mat. Interfaces 8 (2016) 22113–22126.
[34] M. Muñoz-Úbeda, S.K. Misra, A.L. Barrán-Berdón, S. Datta, C. Aicart-Ramos, P. Castro-Hartmann, P. Kondaiah, E. Junquera, S. Bhattacharya, E. Aicart, How does the spacer length of cationic Gemini lipids influence the lipoplex formation with plasmid DNA? Physicochemical and biochemical characterizations and their relevance in gene therapy, Biomacromolecules 13 (2012) 3926–3937.
[35] I.Y. Abdurakhmonov, RNA Interference, IntechOpen, Rijeka, 2016.
[36] R. Zana, Gemini surfactants, in: Novel Surfactants, CRC Press, 2003, pp. 403–442.
[37] M. Martínez-Negro, N. Sánchez-Arribas, A. Guerrero-Martínez, M.L. Moyá, C.T. de Ilarduya, F. Mendicuti, E. Aicart, E. Junquera, A non-viral plasmid DNA delivery system consisting on a lysine-derived cationic lipid mixed with a fusogenic lipid, Pharmaceutics 11 (2019) 632.
[38] M. Martínez-Negro, L. Blanco-Fernández, P.M. Tentori, L. Pérez, A. Pinazo, C.T. de Ilarduya, E. Aicart, E. Junquera, A Gemini cationic lipid with histidine residues as a novel lipid-based gene nanocarrier: a biophysical and biochemical study, Nanomaterials 8 (2018) 1061.
[39] R.-C. Su, Q. Liu, W.-J. Yi, L.-T. Zheng, Z.-G. Zhao, Lipoic acid functionalized amino acids cationic lipids as gene vectors, Bioorg. Med. Chem. Lett. 26 (2016) 4692–4697.
[40] M. Redza-Dutordoir, D.A. Averill-Bates, Activation of apoptosis signalling pathways by reactive oxygen species, Biochim. Biophys. Acta – Mol. Cell Res. 1863 (2016) 2977–2992.
[41] V. Nogueira, N.J.C.C.R. Hay, Molecular pathways: reactive oxygen species homeostasis in cancer cells and implications for cancer therapy, Clin. Cancer Res. 19 (2013) 4309–4314.
[42] P. Poncelet, I. Besson-Faure, T. Lavabre-Bertrand, Clinical applications of quantitative immunophenotyping. Immunophenotyping, J. Wiley & Sons, Toronto, Canada, 2000.
[43] N. Sánchez-Arribas, M. Martínez-Negro, E.M. Villar, L. Pérez, E. Aicart, P. Taboada, A. Guerrero-Martínez, E. Junquera, Biocompatible nanovector of siRNA consisting of arginine-based cationic lipid for gene knockdown in cancer cells, ACS Appl. Mat. Interfaces 12 (2020) 34536–34547.
[44] N. Sánchez-Arribas, M. Martínez-Negro, E.M. Villar, L. Pérez, J. Osío Barcina, E. Aicart, P. Taboada, A. Guerrero-Martínez, E. Junquera, Protein expression knockdown in cancer cells induced by a Gemini cationic lipid nanovector with histidine-based polar heads, Pharmaceutics 12 (2020) 791.
[45] A. Kroll, C. Dierker, C. Rommel, D. Hahn, W. Wohlleben, C. Schulze-Isfort, C. Göbbert, M. Voetz, F. Hardinghaus, J.J.P. Schnekenburger, Cytotoxicity screening of 23 engineered nanomaterials using a test matrix of ten cell lines and three different assays, Part. Fibre Toxicol. 8 (2011) 1–19.
[46] T. Xia, M. Kovochich, M. Liong, J.I. Zink, A.E.J.A. Nel, Cationic polystyrene nanosphere toxicity depends on cell-specific endocytic and mitochondrial injury pathways, ACS Nano 2 (2008) 85–96.
[47] E. Fröhlich, C. Meindl, E. Roblegg, A. Griesbacher, T.R.J.N. Pieber, Cytotoxity of nanoparticles is influenced by size, proliferation and embryonic origin of the cells used for testing, Nanotoxicology 6 (2012) 424–439.
[48] A. Elouahabi, J.-M.-J.-M. Ruysschaert, Formation and intracellular trafficking of lipoplexes and polyplexes, Mol. Ther. 11 (2005) 336–347.
[49] L. Pelkmans, D. Puntener, A.J. Helenius, Local actin polymerization and dynamin recruitment in SV40-induced internalization of caveolae, Science 296 (2002) 535–539.
[50] S.E. Gratton, P.A. Ropp, P.D. Pohlhaus, J.C. Luft, V.J. Madden, M.E. Napier, J. M. DeSimone, The effect of particle design on cellular internalization pathways, Proc. Natl. Acad. Sci. U. S. A. 105 (2008) 11613–11618.
[51] T. Channels, Permeability of muscle capillaries to small heme-peptides, J. Cell Biol. 64 (1975) 586–607.
[52] D.X. Liu, A. Mori, L. Huang, Role of liposome size and RES blockade in controlling biodistribution and tumor uptake of GM1-containing liposomes, BBA 1104 (1992) 95–101.
[53] A. Gabizon, D. Papahadjopoulos, The role of surface-charge and hydrophilic groups on liposome clearance in vivo, BBA 1103 (1992) 94–100.
[54] H.S. Kruth, N.L. Jones, W. Huang, B. Zhao, I. Ishii, J. Chang, C.A. Combs, D. Malide, W.-Y. Zhang, Macropinocytosis is the endocytic pathway that mediates macrophage foam cell formation with native low density lipoprotein, J. Biol. Chem. 280 (2005) 2352–2360.
[55] L.-H. Wang, K.G. Rothberg, R. Anderson, Mis-assembly of clathrin lattices on endosomes reveals a regulatory switch for coated pit formation, J. Cell Biol. 123 (1993) 1107–1117.
[56] I.M. Degors, C. Wang, Z.U. Rehman, I.S. Zuhorn, Carriers break barriers in drug delivery: endocytosis and endosomal escape of gene delivery vectors, Accounts Chem. Res. 52 (2019) 1750–1760.
[57] A.I.J.E. Ivanov, Pharmacological inhibition of endocytic pathways: is it specific enough to be useful? Methods Mol. Biol. (2008) 15–33.
[58] N. Chaudhary, G.A. Gomez, M.T. Howes, H.P. Lo, K.-A. McMahon, J.A. Rae, N. L. Schieber, M.M. Hill, K. Gaus, A.S. Yap, Endocytic crosstalk: cavins, caveolins, and caveolae regulate clathrin-independent endocytosis, PLoS Biol. 12 (2014) e1001832.
[59] A. Verma, O. Uzun, Y. Hu, Y. Hu, H.-S. Han, N. Watson, S. Chen, D.J. Irvine, F. Stellacci, Surface-structure-regulated cell-membrane penetration by monolayer-protected nanoparticles, Nat. Mater. 7 (2008) 588–595.
[60] M.C. Pedroso, S. Simoes, P. Pires, R. Gaspar, V. Slepushkin, N. Duzgunes, Gene delivery mediated by cationic liposomes: from biophysical aspects to enhancement of transfection, Mol. Membr. Biol. 16 (1999) 103–109.
[61] G. Caracciolo, F. Cardarelli, D. Pozzi, F. Salomone, G. Maccari, G. Bardi, A. L. Capriotti, C. Cavaliere, M. Papi, A. Lagana, Selective targeting capability acquired with a protein corona adsorbed on the surface of 1,2-dioleoyl-3-trimethylammonium propane/DNA nanoparticles, ACS Appl. Mat. Interfaces 5 (2013) 13171–13179.
[62] D. Niculescu-Duvaz, J. Heyes, C.J. Springer, Structure-activity relationship in cationic lipid mediated gene transfection, Curr. Med. Chem. 10 (2003) 1233–1261.
[63] S. Motta, V. Rondelli, L. Cantu, E. Del Favero, M. Aureli, D. Pozzi, G. Caracciolo, P. Brocca, What the cell surface does not see: the gene vector under the protein corona, Colloids Surf. B 141 (2016) 170–178.
[64] C. Leal, K.K. Ewert, R.S. Shirazi, N.F. Bouxsein, C.R. Safinya, Nanogyroids incorporating multivalent lipids: enhanced membrane charge density and pore forming ability for gene silencing, Langmuir 27 (2011) 7691–7697.
[65] C. Leal, N.F. Bouxsein, K.K. Ewert, C.R. Safinya, Highly efficient gene silencing activity of siRNA embedded in a nanostructured gyroid cubic lipid matrix, JACS 132 (2010) 16841–16847.
[66] M. Muñoz-Úbeda, S.K. Misra, A.L. Barrán-Berdón, C. Aicart-Ramos, M.B. Sierra, J. Biswas, P. Kondaiah, E. Junquera, S. Bhattacharya, E. Aicart, Why is less cationic lipid required to prepare lipoplexes from plasmid DNA than linear DNA in gene therapy? JACS 133 (2011) 18014–18017.
[67] A.L. Barrán-Berdón, M. Muñoz-Úbeda, C. Aicart-Ramos, L. Pérez, M.R. Infante, P. Castro-Hartmann, A. Martín-Molina, E. Aicart, E. Junquera, Ribbon-type and cluster-type lipoplexes constituted by a chiral lysine based cationic Gemini lipid and plasmid DNA, Soft Matter 8 (2012) 7368–7380.
[68] J. Briggs, H. Chung, M. Caffrey, The temperature-composition phase diagram and mesophase structure characterization of the monoolein/water system, J. Phys. II (6) (1996) 723–751.
[69] S. Tassler, B. Dobner, L. Lampp, R. Ziółkowski, E. Malinowska, C. Wölk, G.J. L. Brezesinski, DNA delivery systems based on peptide-mimicking cationic lipids—the effect of the co-lipid on the structure and DNA binding capacity, Langmuir 35 (2019) 4613–4625.
[70] P. Lu, V.M. Weaver, Z. Werb, The extracellular matrix: a dynamic niche in cancer progression, J. Cell Biol. 196 (2012) 395–406.
[71] M.W. Tibbitt, K.S. Anseth, Hydrogels as extracellular matrix mimics for 3D cell culture, Biotechnol. Bioeng. 103 (2009) 655–663.
[72] L.G. Griffith, M.A. Swartz, Capturing complex 3D tissue physiology in vitro, Nat. Rev. Mol. Cell Biol. 7 (2006) 211–224.
[73] D.L. Sackett, J. Wolff, Nile red as a polarity-sensitive fluorescent probe of hydrophobic protein surfaces, Anal. Biochem. 167 (1987) 228–234.
[74] V. Domínguez-Arca, R.R. Costa, A.M. Carvalho, P. Taboada, R.L. Reis, G. Prieto, I. Pashkuleva, Liposomes embedded in layer by layer constructs as simplistic extracellular vesicles transfer model, Mater. Sci. Eng. C Mater. Biol. Appl. 121 (2021) 111813.